Density functional simulations of noble-gas impurities in diamond

J. P. Goss, R. J. Eyre, and P. R. Briddon
School of Natural Sciences, University of Newcastle Upon Tyne, Newcastle Upon Tyne NE1 7RU, United Kingdom

Alison Mainwood
Physics Department, King's College London, Strand, London WC2R 2LS, United Kingdom

(Received 6 May 2009; revised manuscript received 15 July 2009; published 26 August 2009)

Noble-gas species are important impurities in the geological analysis of natural diamond and are also used in ion implantation on the basis of chemical inertness. We present the results of density functional simulations of noble-gas atoms in diamond. We show that interstitial species are relatively mobile under geological conditions but require annealing above ~700 K for laboratory-based experiments. In addition, with the exception of interstitial helium and neon, the noble-gas atoms are able to react chemically with the diamond due to the compact diamond lattice. This is of particular significance in terms of ion implanted material where noble-gas species trapped in lattice vacancies are electrically active and stable to high temperatures.

DOI: 10.1103/PhysRevB.80.085204 PACS number(s): 61.72.−y, 71.55.Cn

I. INTRODUCTION

Noble gases, especially He and Ar, are used for control experiments in ion-implantation doping[1–3] because once incorporated, it is thought that implanted atoms only weakly perturb the material characteristics. Noble-gas atoms including helium and argon are also detected in natural diamond with isotope effects elucidating the geological history.[4–6] There are three sources of helium in natural diamond: (1) during growth; (2) α-particle implantation from radioactive decay of uranium or thorium in neighboring rocks; and (3) cosmic-ray spallation.

The origins of helium may be separated via isotopic differences. Helium dissolved during growth has the same isotope ratio as the mantle, 4–6 Ra,[7] and is evenly distributed through the crystal. In contrast, the penetration of α particles depends on the energy of the decay but is not more than 10 μm and this process produces ^{3}He:^{4}He of ~0.01 Ra. Finally, cosmic rays penetrate right through the diamond and the spallation reactions with C or N produce ^{3}He:^{4}He ratios of 0.2 to 1. This cosmogenic source is present only when the diamond resides near the surface of the earth, such as where it lies in an alluvial deposit, and produces ~100 helium atoms per gram of diamond per year at sea level.[8,9]

Hence, accurately determining the isotope ratio discriminates between, for example, alluvial diamonds and those from mined kimberlite pipes, and may indicate something of the history of the diamond. In practice, diamonds have helium isotope ratios in the range from below 1 Ra (predominantly radiogenic) to above 200 Ra (predominantly cosmogenic).

The experimental extraction of helium is performed in a high-temperature furnace capable of heating the diamond to 2000 °C (i.e., above the graphitization threshold) and collecting the emitted gas in a mass spectrometer. In some cases the helium isotope ratio decreases by during extraction, implying either a difference in diffusivity of ^{3}He and ^{4}He, or an anisotropic distribution of He isotopes in the original sample.

Diffusion barriers are estimated at 1.02 ± 0.21, 1.08 ± 0.05, and 1.56 eV (Refs. 10–12) but the observations vary widely with sample[11] and isotope. In one study[13] ^{3}He was effused at 500 °C whereas ^{4}He required 1700 °C. In a different study, the effect was reversed, with ^{3}He being much more retentive.[12] The inconsistency may suggest that the diffusion being measured is affected by additional interactions, such as with lattice damage. Indeed, material implanted with 1 meV ^{4}He$^+$ ions[14] shows no diffusion of He in the absence of graphitization or cracking. It is therefore important to determine the diffusion barriers for atomistic mechanisms from accurate quantum-chemical methods.

Despite the use of inert gas ion implantation and its significance in geological analysis, there is little detailed atomistic modeling for the properties of the candidate structures, such as interstitial noble-gas atoms. Therefore, we present the results of first-principles calculations within the density functional approach of the structure, vibrations, electronic structure, and diffusion characteristics of the noble gases He, Ne, Ar, Kr, and Xe in diamond. We first outline the method in Sec. II, report the results in Sec. III, and finally conclude in Sec. IV.

II. METHOD

Calculations were carried out using the local spin-density functional technique,[15] implemented in AIMPRO (Refs. 16 and 17) (*ab initio* modeling program). Simple cubic, 64 and 216 atom supercells of side length $2a_0$ and $3a_0$, along with 256 atoms, body-centered-cubic cells encapsulate the defects. The cell-size dependence may be determined by calculating differences in the formation energies, a value which depends only on the chemical potential of carbon. The level of convergence is known to depend on the volume displaced by the impurity.[18] In the current systems the differences in the formation energies of substitutional He and Ar in between the 64 and 216 atom supercells are 0.1 and 0.2 eV, respectively. Values presented from simulations using the larger supercells are therefore expected to be converged with respect to the cell size to within a few tenths of an eV, the error increasing with the atomic number of the impurity. In all cases, we find that there are no qualitative differences

(e.g., in terms of the chemical reconstructions) between structures in different cell sizes.

The Brillouin zone is sampled using the Monkhorst-Pack scheme,[19] generally with a mesh of $2\times2\times2$ special k points. For representative cases we compare total energies with a finer mesh and the results suggest our values from the coarser mesh are well converged. Core electrons are eliminated using norm-conserving pseudopotentials.[20]

The wave-function basis consists of atom-centered Gaussians.[21] For the carbon(silicon) atoms, independent s and p Gaussians with four widths plus one(two) further set of d Gaussians are used. For the noble-gas atoms we use independent sets of s, p, and d Gaussians with four widths, except for helium where six independent sets of s and p Gaussians are employed. The charge density is Fourier transformed using plane waves with a cutoff of 300 Ry, yielding total energies converged to ~1 meV. The lattice constant and bulk modulus are within ~1 and 5%, respectively, of experimental values while the direct and indirect band gaps at 5.68 and 4.26 eV, respectively, are close to previously published plane-wave values.[22]

The zero-temperature formation energy of a system X in charge-state q may be calculated using

$$E^f(X,q) = E(X,q) - \sum \mu_i + q(E_v^X + \mu_e). \tag{1}$$

Here E is the total energy, μ_i and μ_e are the chemical potentials[23] of the atoms and electrons, respectively, and E_v^X is the energy of valence-band top. Donor or acceptor electrical levels may be estimated using the formation energy method or by use of the marker method.[21,24,25] Electrical levels are of a semiquantitative nature, with error bars of several tenths of an eV resulting from the effects of charged supercells and interactions from their periodic images. However, the calculations are able to place electrical levels in a qualitative nature, such as "mid gap," high or low in the band gap, or close to a band edge. We define a binding energy by $E^b(XY)=E^f(X)+E^f(Y)-E^f(XY)$.

The chemical potential of atomic gas is given by[26]

$$\mu_{\mathrm{X(gas)}} = H_{\mathrm{X}} + k_B T \ln\left\{\left(\frac{p}{k_B T}\right)\left(\frac{2\pi\hbar^2}{m_{\mathrm{X}} k_B T}\right)^{3/2}\right\}, \tag{2}$$

where H_{X} is the enthalpy of the atom as calculated by obtaining the energy of a single noble-gas atom, k_B is the Boltzmann's constant, p is the gas pressure, m_{X} is the mass, and $\hbar$ is the Planck's constant divided by 2π. For the case of hydrogen solubility in diamond, the temperature-dependent component of the chemical potential has been shown to be rather insignificant.[26]

For solids where the pV term is normally small, the Helmholtz free energy (i.e., a constant volume constraint), which is the more natural computational quantity, is a very good approximation for the Gibbs function. The temperature-dependent free energy deviates from the zero-temperature value principally due to entropic terms for heavy species but there may be important contributions for light species arising from vibrational contributions.[27] The vibrational contribution to the free energy of each system under a harmonic approximation may be obtained using[27]

$$F_{\mathrm{vib}}(T) = k_B T \int_0^\infty \{\ln[\sinh(\hbar\omega/2k_B T)]\} g(\omega) d\omega, \tag{3}$$

where $g(\omega)$ is the phonon density of states. The integral is approximated by a sum over the zone-center normal modes, which we obtain by constructing the dynamical matrix using a finite-difference approximation for the force derivative when displacing atoms by 0.1 Å in each of the x, y, and z directions, and then diagonalizing to find the normal modes in the usual way. The total Helmholtz free energy is then given by

$$F = E^f + F_{\mathrm{vib}} - TS_{\mathrm{config}}, \tag{4}$$

where the configurational entropy per impurity term is $k_B \ln(\Omega)/[X]$, with Ω being the enumeration of possible arrangements of the impurity species.

Finally, activation energies for atomic motion have been obtained using the standard climbing nudged-elastic-band (NEB) method.[28,29] Initially approximate profiles are obtained using the well-optimized end points for the reaction or diffusion process without a climbing image. These are then followed by simulations where the highest energy image is allowed to climb and optimization of the minimum-energy path proceeds until the saddle-point energy changes by less than 10 meV between subsequent iterations and the image forces are all less than 10^{-3} atomic units. In addition, the number of images are increased until for a given process the saddle-point energy is found to be independent of this number (typically on the order of 10 images).

III. RESULTS

A. Interstitial He

Supercells were relaxed containing 64 and 216 host sites and a single He atom located initially at high-symmetry sites: the tetrahedral interstitial site (T) and the hexagonal interstitial site (H). Subsequent to the constrained relaxation, the atom positions were randomly perturbed by ~0.1 Å and the structures rerelaxed.

From these calculations we conclude that the ideal T site as most stable. In this form the helium nucleus lies 1.58 Å from the four equivalent nearest C neighbors. These nearest-neighbor carbon atoms are pushed outward in a breathing mode, resulting in three extended C-C bonds (1.57 Å) and one compressed (1.50 Å).

The constrained H-site structure, which is 2.3 eV above the ground state, also yields He-C internuclear distances of 1.57 Å with the C-C bonds in the hexagonal ring dilated at 1.63 Å. The H structure possesses a single imaginary mode, which points along $\langle111\rangle$ and combined with NEB calculations we conclude that He_i diffuses by hops between T sites via H sites with a barrier of 2.3 eV.

To shed further light upon this barrier, and noting that the diffusion barrier of He_i in Si is much lower at 0.6 ± 0.1 eV,[10] we have also calculated the diffusion barrier for He_i in silicon. We find a diffusion barrier 0.7 eV in excellent agreement with the experimental determination. We conclude that our computational method is reliable and

TABLE I. Local vibrational mode frequencies (cm^{-1}) for helium in diamond. The irreducible representations are indicated in parentheses.

Structure	Symmetry	Isotope	Frequency (symmetry)	
T	T_d	^{3}He	1365 (A_1)	1651 (T_2)
T	T_d	^{4}He	1365 (A_1)	1483 (T_2)
H	D_{3d}	^{3}He	1395 (A_{1g})	2109 (E_u)
H	D_{3d}	^{4}He	1395 (A_{1g})	1869 (E_u)

hence the relatively high value computed for diamond is probably correct.

The impact of a high He_i diffusion barrier may be modeled as an Arrhenius process. For the attempt frequency, ν_a, we may use the calculated local modes of He_i, listed in Table I, or calculate an attempt frequency based on Vineyard's theory.[30] In the current case, $\nu_a(^3\text{He})=485\ \text{cm}^{-1}$ and $\nu_a(^3\text{He})=422\ \text{cm}^{-1}$, around 30% of the respective local-mode frequencies. This reflects the relatively higher frequencies at the saddle point.

The Arrhenius relation yields an expression for the temperature

$$T = E^a/k_B[\ln(\nu_a/\nu)]. \tag{5}$$

where ν is the hop rate, E^a is the activation barrier, and ν_a is the attempt frequency. The logarithmic dependence on ν_a renders resultant temperature relatively insensitive to the isotope and whether we use the local mode or Vineyard theory. A hop rate characteristic of laboratory-based experiments on the order of 1 Hz would require a temperature above ~880 K using ν_a from the Vineyard theory calculation. Allowing for a ±0.2 eV error bar in the activation energy provides an estimate of the error bar for this temperature at around ±80 K.

However, in a geological context time scales may be billions of years[31] with temperatures above 1000 °C.[32,33] To put this into context, for $T=1000$ °C, $\nu_a=14$ THz (from the Vineyard calculation), and $E^a=2.3$ eV, ν is on the order of 10 kHz. This implies interstitial helium would be very mobile in crystalline diamond during its geological residence.

It is important to compare the calculated value with those obtained from high-temperature annealing experiments, which lie in the 1.0–1.5 eV range. This may be a consequence of the measured activation energies corresponding to a different process, such as diffusion of He_i through defective diamond at the onset of graphitization. Indeed, such a low barrier seems inconsistent with the presence of helium dissolved in the diamond persisting to the high temperatures and long times experienced in the geological context.

Finally, we estimate an approximate solubility for He_i in diamond. In the context of this calculated value we are estimating the equilibrium concentration in a diamond under annealing conditions where the He assumed to be in equilibrium with He gas. It is not an estimate of the concentration of He expected in equilibrium with a geological growth environment. The zero-temperature formation energy of ^4He_i is 6.5 eV, of which ~230 meV is zero-point vibrational contribution. Thus, at $T=0$ K, the solubility of He_i is practically nil. The temperature-dependent terms in Eq. (4) all tend to increase the solubility and the calculated temperature dependency is shown in Fig. 1.

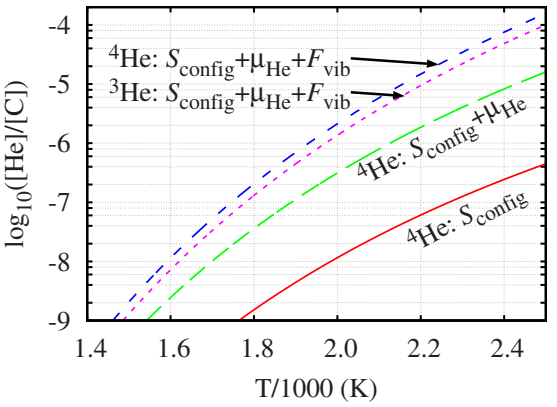

FIG. 1. (Color online) Solubility of He_i in diamond for a He gas pressure of 1 atmosphere, as described in the text. The solid (red) line includes only the configurational entropy for ^{4}He; the long-dashed (green) line also includes variation in μ_{He}; the short-dashed (blue) line also includes F_{vib}, and the dotted (magenta) line shows the total solubility for ^{3}He.

At high temperatures the calculated solubility becomes relatively large. However, we find that He_i is relatively mobile, even at 900 K. The equilibrium concentration of He_i at 2000 K may be several parts per million. If cooling does not occur sufficiently quickly the concentration would drop rapidly and be well below parts per trillion before He_i is frozen in supersaturation within an otherwise perfect diamond lattice. If, on the other hand, cooling is very rapid all helium dissolved or radiated into the diamond while it is deep under the earth's crust may be frozen in until mined. Indeed, the time resident in the geological layers from which the samples are obtained will also impact upon whether the helium remains within the diamond—prolonged anneals at a few 100 °C would be sufficient over the potentially long periods to allow the He to migrate.

B. Substitutional He

Implanted helium, including radiogenic sources, may result in helium lying on a carbon site. Given the size and nonreactive nature of noble gases, such a defect may be viewed as a complex of a lattice vacancy with He_i.

Relaxation has been performed from various starting structures. From our analysis, we find that the energetically preferred geometry has C_{2v} symmetry, as shown in Fig. 2(b). The helium atom is closer to two carbon neighbors (He-C distances of 1.44 Å) with two more distant carbon neighbors at 2.09 Å. This is 1.6 eV lower in energy than where the helium atom is constrained to lie on the lattice site (four He-C distances of 1.83 Å). However, it is known that multiplet effects play an important role in diamond and, in particular, in the neutral vacancy,[34,35] which is similar to the on-site He_s center. Nevertheless, since the multiplet splittings in V are of the same order as the 1.6 eV relaxation energy we

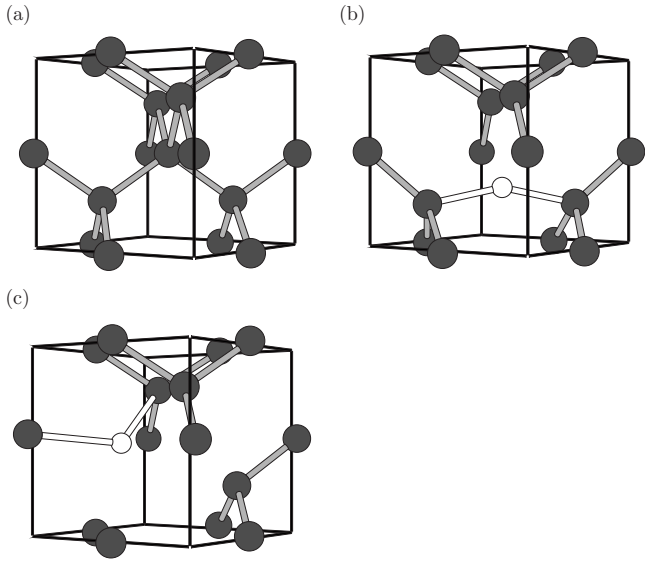

FIG. 2. Schematics of (a) bulk diamond, (b) He_s, and (c) He_s-V in diamond. Gray and white atoms are C and He, respectively, and the cubes indicate the underlying cubic axes. White bonds indicate the nearest neighbors to helium in each case.

report for He_s, they are unlikely to significantly affect the relative stabilities of He_s and He_i discussed below. In the C_{2v} structure, there are four defect states in the band gap, characterized by the electronic configuration $a_1^2 b_1^2 b_2^0 a_1^0$.

Regardless of the detailed structure of He_s the center results in empty gap levels, suggesting that He_s may accept electrons. By comparison with the known acceptor level of the vacancy-nitrogen complex at $E_c-2.583$ eV (Ref. 36) as a marker,[21] the distorted structure [Fig. 2(b)] possesses an acceptor level at $E_c-2.5$ eV and we conclude that He_s may act as a mid-gap acceptor. This has obvious implications for electrical conductivity.

He_s may be visible due to the light impurity giving rise to vibrational infrared absorption. The orthorhombic He_s has a single, IR-active local vibrational mode, lying at 1522 and 1668 cm^{-1} for ^4He and ^3He, respectively, corresponding to stretching modes of the helium atom between the two nearest carbon atoms. In the likely event of low concentrations of He_s, the direct detection via infrared spectroscopy would be unlikely. However, they may be resolved as local-mode replicas of an electronic transition: the optical transition between the highest-occupied and lowest-unoccupied levels is dipole forbidden but would be rendered allowed with the participation of the local mode. The clear isotopic dependence would be a key characteristic for experimental investigations to elucidate the true structure of He_s since the on-site structure will give riser to lower-frequency modes.

Finally, we present the analysis of the thermal stability of He_s. The binding energy of He_i to a lattice vacancy may be estimated using a combination of the current calculations and the quantum Monte Carlo value for the formation energy of the lattice vacancy.[35] We obtain a value for the binding energy of 2.2 eV. Then, for dissociation into He_i and V, the activation energy, approximated by the sum of the binding and diffusion energies, is 4.5 eV.

Alternatively, He_s may migrate. An estimate of the diffusion energy for exchange of helium with a nearest neighbor from a NEB simulation is found to be just 4.9 eV, lower than calculated[37] for similar processes involving N_s or B_s.

$E^f(He_s) > E^f(He_i)$ so that *in equilibrium* $[He_s] \ll [He_i]$. The estimated diffusion barrier for He_s is comparable to the experimentally inferred activation energy for N_s aggregation into A centers.[38,39] In most natural diamond, conversion from N_s into A centers is typically complete. Therefore, provided that the helium is introduced onto a substitutional site with sufficient time for the annealing process to occur geologically, we expect the trapping of He_i at a lattice vacancy to form He_s is unlikely to survive. If the He is implanted (cosmogenic) while the diamond is near the surface of the earth, the large binding energy and relatively high migration barrier may render these centers kinetically stable.

C. He_s-vacancy complexes

As shown above, we find a relatively low thermal stability of He_s and He_i. Taking the view that helium may be stabilized if more space is afforded to it and taking He_s to be effectively a complex of a monovacancy and He_i, we have also examined complexes made up from He_i and multiple vacancies.

We start with the simple, nearest-neighbor divacancy and add the noble-gas atom. As with the monovacancy case (He_s) helium energetically prefers the proximity of carbon atoms, Fig. 2(c), rather than residing at the center of the divacancy, the structure preferred by a large number of impurity species.[40] However, the split-vacancy structure where helium is equidistant to six equivalent carbon neighbors is just 0.2 eV higher in energy, indicating a much weaker interaction than for He_s.

The trend extends to larger voids. As a prototypical system we place helium in a ring hexavacancy.[41] (We particularly do not suppose that natural or synthetic diamonds contain these specific vacancy aggregates but use this structure as a larger space in which to place the noble-gas species but which remains a defect which can legitimately be regarded as pointlike. We note however that there is evidence that nanosized voids are present in diamond.[42,43]) In the case of helium at the core of the hexavacancy, we find the complex to be 2.3 eV *lower* in energy than when in a metastable, chemically interacted structure (similar to that found for He_s and He_s-V).

An important difference between the different sized voids is seen in the variation in the electron densities in the "empty" regions. The calculated variations along the C_3 $\langle 111 \rangle$ axes of the monovacancy, divacancy, and hexavacancy are plotted in Fig. 3.

The charge density at the center of the hexavacancy is an order of magnitude lower than the monovacancy and divacancy. Then, in larger voids the helium atoms can adopt locations where there is a much lower charge density and hence a reduced overlap between the helium wave functions and the diamond host. However, for the small voids, such as a monovacancy, no such site exists and there is an energetic expedient to the chemical reaction of the noble-gas atom with the diamond host.

89% of the zero-temperature formation energy of He_i is liberated by placing it at the center of a hexavacancy and the

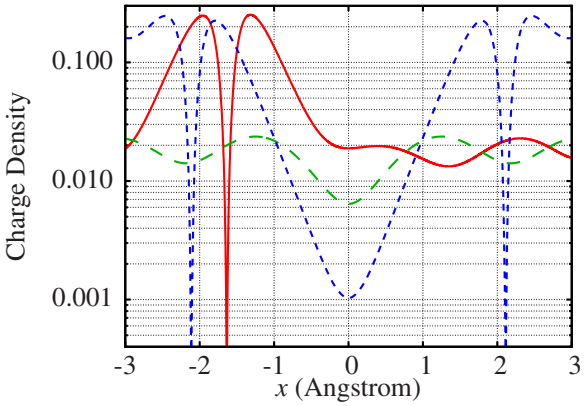

FIG. 3. (Color online) Charge density (atomic units) along ⟨111⟩ axes of the monovacancy (solid line), divacancy (dashes), and hexavacancy (dots). The center of symmetry is at $x=0$ Å in each case.

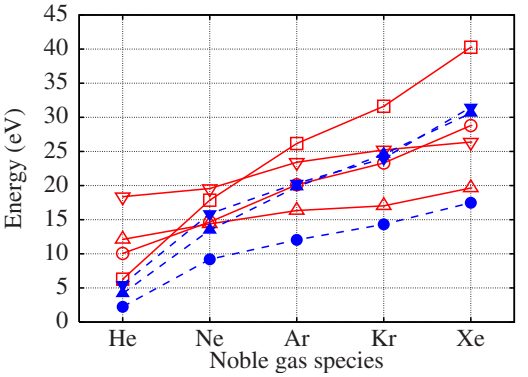

FIG. 4. (Color online) Calculated formation energies (empty symbols) and binding energies (filled symbols) for noble-gas centers in diamond (eV): $E^f(X_i)$ ■; $E^f(X_s)$ ○; $E^f(X_i-V_2)$ △; $E^f(X_i-V_6)$ ▽; $E^b(X_i,V)$ ●; $E^b(X_i,V_2)$ ▲; and $E^b(X_i,V_6)$ ▼.

barrier to dissociation of V_6-He is around 8 eV, a large value even in a geological context. We therefore conclude that even relatively small voids may be sufficient to stabilize He within diamond and that structures of this type may be responsible for the measured release of He from natural diamonds at high temperatures.

D. Other noble-gas impurities

The properties of helium may be put into further context by comparison with other noble-gas species. Table II lists the formation energy and diffusion barriers calculated for He, Ne, Ar, Kr, and Xe. We note that in practice noble-gas species are most likely introduced into the diamond via implantation processes. However, once incorporated in such nonequilibrium mechanisms, formation energies provide some insight into the likelihood of the species being retained or diffusing out of the diamond during annealing processes.

Structurally, interstitial noble-gas species are found to be stable in one of two distinct forms. For the smaller species of He and Ne, the T site is preferred and both migrate via the H site.

In contrast, Ar, Kr, and Xe all *chemically react* with the lattice and form [001]-oriented split interstitials. The reaction is highly exothermic so that the split-interstitial configuration is 10.8, 13.6, and 14.2 eV lower in energy than the T site for Ar, Kr, and Xe, respectively. Despite the qualitatively different structure, the larger noble gases are also found to migrate with low barriers. The trajectory is via a through-bond mechanism also found for interstitial nitrogen.[44] The diffusion barriers range from 3.0 to 3.7 eV, corresponding to a temperature range of 1100–1400 K for $\nu=1$ Hz and ν_a around the one-phonon maximum of the host material [Eq. (5)]. Thus, over geological time scales and temperatures, species such as Ar_i should be considered as mobile.

We have compared Ar_i in diamond with the analogous cases in silicon where Ar does not exhibit any tendency to react with the lattice. The qualitative difference between Si and diamond can be understood as follows. The potential well in which a nonbonded Ar_i site confines the atomic wave functions, raising their energy. For Ar_i at the T site in diamond, this results in a mid-gap level principally comprised of the Ar $3p$ electrons. The total energy is then able to be reduced by rehybridization of these electrons following reaction with the lattice. In contrast, the reduced confinement at the T site in silicon results in no gap levels and then there is no energetic expedient for any chemical reaction.

Figure 4 shows a trend in formation energy with atomic number. Even allowing for a temperature dependence of the solubility from Eq. (4), the solubility of interstitial helium is

TABLE II. Summary of zero-temperature formation (E^f) and migration (E^a) energies (eV) calculated for interstitial noble-gas species in diamond. Energies are from 216-host site supercells and the chemical potentials of the noble-gas impurities are taken from isolated atoms. The migration trajectories are indicated, where T, H, split, and BC refer to the T site, H site, [001]-split interstitial, and bond-centered configurations, respectively. $\Delta E=E^f(X_i)-E^f(X_s)$ is positive for species which are more thermodynamically stable as substitutional species.

Species	Structure	$E^f(T=0)$	E^a	Route	ΔE
He	T site	6.3	2.35	T–H–T	−3.8
Ne	T site	17.9	1.56	T–H–T	3.2
Ar	Split	26.2	3.04	Split–BC–split	6.0
Kr	Split	31.6	3.13	Split–BC–split	8.3
Xe	Split	40.3	3.72	Split–BC–split	11.5

greater than all other species we investigated by many orders of magnitude.

For the substitutional site, we find that all noble-gas species react with the lattice in a similar fashion to that described above for He: Ar_s, Kr_s, and Xe_s gain ~0.6 eV by moving off the lattice site, whereas the saving is smaller at ~0.1 eV for Ne_s.

However, there is a very important distinction between helium and all other substitutional noble-gas impurities: *the formation energies of* Ne_s, Ar_s, Kr_s, and Xe_s are less than their interstitial counterparts (ΔE in Table II). The implication is that these noble-gas species would be present in diamond preferentially in association with monovacancies, especially in the context of ion implantation. This trend is extended in terms of the larger voids so that for Ar, Kr, and Xe the interstitial site is less favorable than within the divacancy or hexavacancy, *even including their large formation energies*.

To place this on a more quantitative basis, we have calculated the diffusion barrier for concerted exchange for Ar_s, obtaining a value of 5.9 eV. In the case of the annealing of He_s, we predict that the diffusion could take the form either of dissociation or concerted migration activated by 4.5–4.9 eV. However, since Ar_s is more stable than Ar_i, it is the 5.9 eV diffusion barrier of Ar_s that limits its stability.

Binding energies (Fig. 4) rapidly increase with atomic number and cavity size. For the ring hexavacancy, with the possible exception of He, the void represents a deep trapping site, even on a geological scale: the energy required to move Ne_i from a hexavacancy to a distant interstitial site is 17 eV, with larger values for Ar, Kr, and Xe.

The large formation energies shown in Fig. 4 indicate the low probability of formation under equilibrium conditions. However, ion implantation is highly nonequilibrium and formation of vacancy-impurity complexes is both likely and will require high-temperature annealing to be reversed.

Finally, we note that although the cage-site interstitials (He and Ne) are electrically inactive, the split interstitials, Ar_i, Kr_i, and Xe_i possess occupied electronic states within the diamond band gap. Using the formation energies, we find that the chemically reacted interstitials possess both donor and acceptor levels in the band gap but relatively close to the band edges in each case. The electrical levels are plotted schematically in Fig. 5. For example, Ar_i has a a donor level estimated at $E_v+0.8$ eV and an acceptor level around 0.5 eV below the conduction band.

In contrast, Ar_s possesses both occupied and empty bands in the gap, leading to an acceptor at $E_v+2.4$ eV and a donor at $E_v+1.6$ eV. Indeed, all substitutional noble-gas defects (also shown in Fig. 5) are electrically active. The levels of the substitutional species show clear trends, a consequence of the common origin, being gap states derived from the four carbon sites immediately adjacent to the impurity. The noble-gas impurities in multivacancies also result in levels in the band gap (not plotted) with electrical levels arising from the chemically unsatisfied carbon atoms at the void surface.[42,43]

Combining the electrical activity with the thermal stability, where high concentrations of these "inert" species are introduced via implantation, they will impact upon the conduction characteristics, in line with a suggested mechanism involving the deep levels of the lattice vacancy.[45] Indeed, this may have been observed in practice with Xe implanted diamond exhibiting apparent *n*-type conductivity,[2] assigned at that time to graphitization.

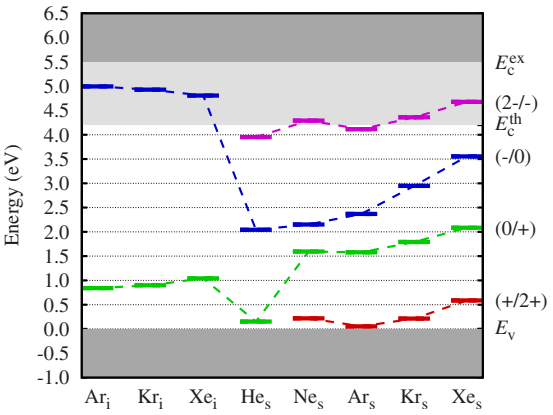

FIG. 5. (Color online) Schematic showing the calculated electrical levels obtained using the μ_e-dependent formation energies of selected interstitial and all substitutional species explored in this study. E_v is the valence-band top, with E_c^{th} and E_c^{ex} being the theoretical and experimental conduction-band minima, respectively. The nature of the electrical transitions, viz., double-acceptor $(2-/-)$, acceptor $(-/0)$, donor $(0/+)$, or double donor $(+/2+)$ is indicated on the right and transitions of the same type are joined with dashed lines.

IV. SUMMARY AND CONCLUSIONS

We have presented the results of density functional simulations of noble-gas impurities in diamond and draw a number of conclusions. First, although one normally considers noble-gas species as chemically nonreactive, in the closely packed environment of the diamond lattice, there is an energetic expedient for the formation of chemical bonds.

In the case of He, although at higher temperatures He_i may be relatively soluble, it remains mobile to modest temperatures where the equilibrium solubility under laboratory annealing conditions is very low. The relative mobility of noble-gas species in diamond suggests that the helium measured in annealing natural diamonds to high temperature are most likely associated with impurities not dissolved in the lattice but rather trapped at voids, inclusions, or other non-diamond regions within the samples.

In experiments performed upon natural diamonds, there is a clear distinction between the diffusion of ^{3}He and ^{4}He. However, we have shown that there is no substantive difference in the diffusion of the two isotopes if they are in the form of, for example, He_i or He_s. Rather, the calculations appear to support the suggestion that the two helium isotopes are inhomogeneously incorporated in these diamonds so that they are then released upon graphitization of the regions containing the noble-gas species. The source of the inhomogeneous incorporation of the helium isotopes remains to be explained.

Finally the role of implanted noble-gas species such as Ar or Xe to produce damage but otherwise leave the material

unaffected cannot be assumed. We find that all noble-gas species are likely to interact strongly with lattice damage, resulting in thermally stable, electrically active centers. Such damage will have to be taken into account in order to understand the electrical and optical properties of the implantation damaged diamond samples.

ACKNOWLEDGMENTS

J.P.G., R.J.E., and P.R.B. gratefully acknowledge the EPSRC for funding. A.M. acknowledges the support of the EU-funded Research Training Network, DRIVE (Grant No. MRTN-CT-2004-512224).

[1] J. O. Orwa, K. W. Nugent, D. N. Jamieson, and S. Prawer, Phys. Rev. B **62**, 5461 (2000).
[2] J. F. Prins, J. Phys. D **34**, 2089 (2001).
[3] E. Trajkov and S. Prawer, Diamond Relat. Mater. **15**, 1714 (2006).
[4] R. Burgess, L. H. Johnson, D. P. Mattey, J. W. Harris, and G. Turner, Chem. Geol. **146**, 205 (1998).
[5] L. H. Johnson, R. Burgess, G. Turner, H. J. Milledge, and J. W. Harris, Geochim. Cosmochim. Acta **64**, 717 (2000).
[6] R. Burgess, E. Layzelle, G. Turner, and J. W. Harris, Earth Planet. Sci. Lett. **197**, 193 (2002).
[7] The Ra unit is the atmospheric ^{3}He:^{4}He ratio, 1.4×10^{-6}.
[8] D. Lal, H. Craig, J. F. Wacker, and R. Poreda, Geochim. Cosmochim. Acta **53**, 569 (1989).
[9] D. Lal, Annu. Rev. Earth Planet Sci. **16**, 355 (1988).
[10] L. C. Luther and W. J. Moore, J. Chem. Phys. **41**, 1018 (1964).
[11] S. Zashu and H. Hiyagon, Geochim. Cosmochim. Acta **59**, 1321 (1995).
[12] R. C. Wiens, D. Lal, W. Rison, and J. F. Wacker, Geochim. Cosmochim. Acta **58**, 1747 (1994).
[13] Yu. A. Shukolyukov, A. M. Pleshakov, and L. D. Lavrova, Petrology **1**, 95 (1993).
[14] J. O. Orwa, D. N. Jamieson, K. W. Nugent, S. Prawer, and R. Kaish, Nucl. Instrum. Methods Phys. Res. B **124**, 515 (1997).
[15] J. P. Perdew and Y. Wang, Phys. Rev. B **45**, 13244 (1992).
[16] R. Jones and P. R. Briddon, in *Identification of Defects in Semiconductors*, Semiconductors and Semimetals Vol. 51A, edited by M. Stavola (Academic, Boston, 1998), Chap. 6.
[17] M. J. Rayson and P. R. Briddon, Comput. Phys. Commun. **178**, 128 (2008).
[18] J. P. Goss, P. R. Briddon, and R. J. Eyre, Phys. Rev. B **74**, 245217 (2006).
[19] H. J. Monkhorst and J. D. Pack, Phys. Rev. B **13**, 5188 (1976).
[20] C. Hartwigsen, S. Goedecker, and J. Hutter, Phys. Rev. B **58**, 3641 (1998).
[21] J. P. Goss, M. J. Shaw, and P. R. Briddon, in *Theory of Defects in Semiconductors*, Topics in Applied Physics Vol. 104, edited by David A. Drabold and Stefan K. Estreicher (Springer, Berlin/Heidelberg, 2007), pp. 69–94.
[22] D. A. Liberman, Phys. Rev. B **62**, 6851 (2000).
[23] The chemical potentials are the Gibbs functions per particle.
[24] J.-W. Jeong and A. Oshiyama, Phys. Rev. B **64**, 235204 (2001).
[25] J. P. Goss, P. R. Briddon, S. J. Sque, and R. Jones, Diamond Relat. Mater. **13**, 684 (2004).
[26] J. P. Goss, R. Jones, M. I. Heggie, C. P. Ewels, P. R. Briddon, and S. Öberg, Phys. Rev. B **65**, 115207 (2002).
[27] S. K. Estreicher, M. Sanati, D. West, and F. Ruymgaart, Phys. Rev. B **70**, 125209 (2004).
[28] G. Henkelman, B. P. Uberuaga, and H. Jónsson, J. Chem. Phys. **113**, 9901 (2000).
[29] G. Henkelman and H. Jónsson, J. Chem. Phys. **113**, 9978 (2000).
[30] G. H. Vineyard, J. Phys. Chem. Solids **3**, 121 (1957).
[31] R. Burgess, G. Turner, and J. W. Harris, Geochim. Cosmochim. Acta **56**, 389 (1992).
[32] F. R. Boyd, J. J. Gumey, and S. H. Richardson, Nature (London) **315**, 387 (1985).
[33] L. M. Barron, S. R. Lishmund, G. M. Oakes, B. J. Barron, and F. L. Sutherland, Austral. J. Earth Sci. **43**, 257 (1996).
[34] C. A. Coulson and M. J. Kearsley, Proc. R. Soc. London, Ser. A **241**, 433 (1957).
[35] R. Q. Hood, P. R. C. Kent, R. J. Needs, and P. R. Briddon, Phys. Rev. Lett. **91**, 076403 (2003).
[36] J. W. Steeds, S. J. Charles, J. Davies, and I. Griffin, Diamond and Related Materials **9**, 397 (2000).
[37] J. P. Goss and P. R. Briddon, Phys. Rev. B **73**, 085204 (2006).
[38] T. Evans, Z. Qi, and J. Maguire, J. Phys. C **14**, L379 (1981).
[39] T. Evans and Z. Qi, Proc. R. Soc. London, Ser. A **381**, 159 (1982).
[40] J. P. Goss, P. R. Briddon, M. J. Rayson, S. J. Sque, and R. Jones, Phys. Rev. B **72**, 035214 (2005).
[41] S. K. Estreicher, J. L. Hastings, and P. A. Fedders, Appl. Phys. Lett. **70**, 432 (1997).
[42] N. Fujita, R. Jones, S. Öberg, and P. R. Briddon, Diamond and Related Materials **18**, 843 (2009).
[43] R. Jones, Diamond and Related Materials **18**, 820 (2009).
[44] J. P. Goss, P. R. Briddon, S. Papagiannidis, and R. Jones, Phys. Rev. B **70**, 235208 (2004).
[45] E. Baskin, A. Reznik, D. Saada, J. Adler, and R. Kalish, Phys. Rev. B **64**, 224110 (2001).